INFLUENCE OF SECONDARY ELECTRON EMISSION ON THE RF GAS BREAKDOWN

A.N. Dakhov, S.V. Dudin
V.N. Karazin Kharkov National University, Kharkov, Ukraine
E-mail: alex.dakhov@gmail.com

The influence of the electron impact secondary electron emission on the RF gas breakdown has been researched experimentally and theoretically with use of particle-in-sell simulation. The experiments and simulations are conducted in the discharge chamber with asymmetric electrodes which is frequently used in technological applications. As a result, the physical mechanism of secondary electron participation in the RF breakdown has been revealed.

PACS: 52.80.Pi

INTRODUCTION

Gas discharge breakdown is one of the most basic problems of gas-discharge physics, which has been studying for more then 100 years [1 - 5]. Nevertheless, despite the long history the breakdown physics is not completely understood and permanently attracts attention of researchers [6 - 12].

The radio frequency (RF) discharge breakdown is very specific case in which oscillatory motion of electrons between electrodes may cause dramatic change of Paschen curve [3, 9]. The breakdown voltage drops significantly comparing to the DC breakdown when the electron oscillation amplitude became less than half of inter-electrode gap. Another unusual feature of the RF breakdown curve is the ambiguity region at low pressures where the discharge can be ignited not only by increase of the RF voltage amplitude but also by the amplitude decrease [3 - 12].

A number of researchers studied features of the RF breakdown curve experimentally and theoretically, so to the moment influence of different factors has been investigated such as kind of gas [8, 9, 11], oscillation frequency [2 - 4, 6, 10], spacing between electrodes [6, 8, 11], discharge chamber geometry [3, 10]. It was also shown experimentally that the electrode surface material has evident impact on the low-pressure part of the RF breakdown curve [8, 9]. The influence was attributed to the electron impact secondary emission and a simple phenomenological model was built giving results consistent with the experimental data. In the paper [13] two kinds of the secondary electron emission were taken into account in one-dimensional particle-in-cell simulation of the RF breakdown, namely the emission induced by electron (*e*-*e*) and ion (*i*-*e*) impact; however, the physical mechanism of the secondary electrons participation in the breakdown process has not been cleared.

The problem with the *e*-*e* secondary emission is that for the first glance it can not play significant role in the RF breakdown since at any phase of the applied RF voltage the electric field brakes either primary or secondary electrons. When the primaries are attracted to an electrode by electric field the produced secondaries are turned back to the electrode due to action of the field. Otherwise, in the reverse phase when the field would accelerate the secondaries outside the electrode the primaries are repelled thereby providing no source for the secondaries.

Experiments and calculations indicate the considerable effect of *e*-*e* emission, so the details of physical processes with the secondary electrons during the RF breakdown are of great interest. Analogous phenomenon is known for decades as multipactor discharge [14-16] where the secondary *e*-*e* emission can provide breakdown of high-vacuum electrode spacing. In the case of very low gas pressure the primary electrons arrival to the electrode in "right" phase occurs due to inertial motion of the electrons accelerated in previous phase of oscillation. However, the RF gas discharge breakdown occurs at relatively high gas pressures when the electron mean free path is much shorter than the electrode spacing, and pure multipactor discharge is impossible due to interruption of the inertial motion by electron-atom collisions.

The main purpose of the present paper is to clarify the physical mechanism of the influence of the secondary *e*-*e* emission on the RF gas breakdown. The optimal way of this problem solution is the combination of experimental research giving authentic information and of numerical simulation allowing to penetrate into fine details of the physical processes. An additional objective is to take into account real discharge chamber geometry, particularly the system with asymmetric electrodes. This requires application of two-dimensional model for the breakdown simulation.

1. EXPERIMENT

The simplified schematic diagram of experimental set-up used in our investigation of the influence of the secondary *e*-*e* emission on the RF gas breakdown is shown in Fig. 1. The discharge was ignited in a cylindrical chamber with inner diameter 12 cm and height 4 cm. The side wall is made of stainless steel grid with the cell size 0.25 mm and optical transparency about 0.5. The RF power is coupled to the stainless steel bottom electrode via a matching box; the top one and side wall are grounded. Such asymmetric design of the electrodes is usually used in technology reactors in order to achieve higher dc bias on the bottom electrode accelerating ions towards the processed surface. The top electrode surface element is replaceable allowing testing surface materials with different secondary electron emission yield. In the described experiments aluminium, stainless steel and graphite were used.

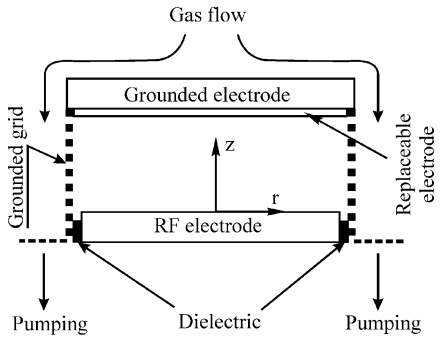

Fig. 1. Schematic diagram of experimental set-up

The electrodes are installed inside a bigger vacuum chamber that allows avoiding any gas pressure gradients inside the discharge volume since the gas feeding and pumping occurs outside. The RF discharge was ignited in argon at pressures in the range p = 20…200 mTorr. The gas pressure is monitored with a capacitance pressure transducer. The system is evacuated by a turbo molecular pump to residual pressure 10^{-5} Torr. The RF power (13.56 MHz) is supplied by an RF generator with maximum output power of 500 W. For the high-pressure part of the breakdown curve the gas pressure was fixed, and then the RF voltage was slowly increased until gas breakdown occurs. The low-pressure part of the curve may be multi-valued, therefore in this range we first decreased the gas pressure, then fixed the RF voltage value and then increased the gas pressure slowly until gas discharge ignition occur. At the moment of the discharge breakdown the RF voltage shows a sharp change, and the ion current appears from a sidewall plane probe located outside the discharge volume sufficiently far from the side wall grid, so not to make any change in the spatial distribution of the electric field. The probe with 1 cm^2 area was biased at -25 V to be at ion saturation part of current-voltage characteristics. The uncertainty in the measured breakdown voltage amplitude U_{br} was no more then 2% over the whole U_{br} range under study.

Fig. 2 shows the breakdown curves of RF discharge in argon measured with the upper electrode made of different materials (aluminium, stainless steel and graphite).

All the used materials were usual technical-grade materials without any special conditioning. As can be seen from the graph two pressure ranges could be distinguished. For high pressures (more then 100 mTorr) the observed breakdown voltages match for the all applicable materials, while at low pressures the discharge curves are significantly affected by the electrode material. It is well known that among the used electrode materials the oxidized aluminium has the lowest work function and the highest electron emission yield while the electron yield from carbon is the lowest [17].

So the Fig. 2 shows that with the increase of the electron emission yield the low-pressure part of the breakdown curve is shifted to the left and a bit down. In all the experimental curves the region of ambiguous dependence of the RF breakdown voltage on the gas pressure is clearly visible at the lowest pressures.

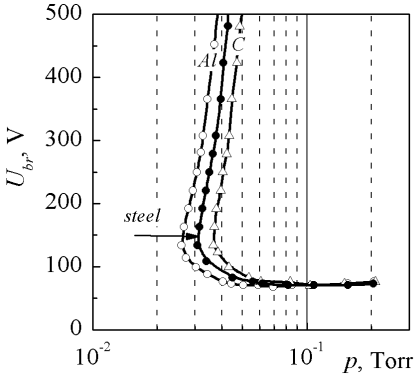

Fig. 2. Dependence of the measured RF breakdown voltage amplitude on argon pressure for different materials of top electrode

2. SIMULATION

2.1. MODEL DESCRIPTION

The simulation was performed using two dimensional particle-in-cell (PIC) model implemented by Tech-X Copr. in OOPIC Pro code [18]. OOPIC Pro is designed to model plasmas, beams of charged particles, externally generated electric and magnetic fields, and low-to-moderate density neutral gases, using a broad variety of boundary and initial conditions. OOPIC Pro includes Monte Carlo collision algorithms for modeling collisions of particles with background gases that might result in the ionization of the background gases and the production of a pre-defined species of particle. The used code considers elastic, excitation and ionization types of the electrons collisions with neutral gas and elastic and charge exchange types of the ion collisions with neutral gas. The simulations were performed for argon gas. Each macro particle included one physical particle. In typical simulation ten thousands particles were used. The uniform gas temperature was set as 0.025 eV. The simulation grid and time steps were chosen reasonably small, that computing process ensures authentic physical results with minimal computing time. The simulation time step should be significantly less than the electron mean free time, than the grid cell crossing time by the fastest particles, and than the RF period. Thus the time step for the simulation was chosen as 10^{-10} s. The grid step was 1 mm. We used electrostatic simulation field solver, so the particle currents are ignored.

To determine the breakdown voltage we used condition of balance between creation of electrons by ionization and secondary emission and their loss to the walls. The breakdown occurs when the electron creation rate exceeds the rate of their loss on the walls. We should take into account that the electrons born in different regions of the discharge chamber and at different phases of driving voltage bring different contribution to the entire particle balance. Thus, in order to consider all the possible variants, as an initial condition of the breakdown we accounted for ionization using random generation of electrons appearing uniformly over the entire volume of the chamber during one period of driving RF voltage. The initial electron creation rate was chosen to ensure the mean equilibrium number of macroparticles in order of 10^4 that provides sufficient simulation accuracy along with acceptable calculation time. For each

value of the gas pressure we searched the RF voltage amplitude providing unchanged mean number of electrons over several RF periods.

Obviously, the particle balance in the discharge chamber is affected both by the appearance of electrons in the chamber volume and the electron emission from the walls. Since the main focus of this paper is the influence of electrode material on the breakdown voltage, special attention was paid to correct description of the secondary electron emission yield.

Vaughan secondary production model is used for electron impact on the electrode surface that includes energy and angular dependence of the emission yield [19]. The secondary electron yield is given by:

$$\delta(\varepsilon,\theta) = \delta_{\max} \cdot (1 + k_s \frac{\theta^2}{2\pi}) \cdot (we^{(1-w)})^k , \quad (1)$$

$$k = \begin{cases} 0.62, w < 1 \\ 0.25, w \geq 1 \end{cases} , \quad (2)$$

$$w = \frac{\varepsilon - \varepsilon_{thr}}{\varepsilon_{\max}\left(1 + k_{sw}\frac{\theta^2}{2\pi}\right) - \varepsilon_{thr}} , \quad (3)$$

where ε is the incident energy of a particle, θ is its angle of incidence measured with respect to the surface normal, k_s is a surface smoothness parameter which was set to 1 for all our simulations, δ_{max} is the peak of the secondary emission coefficient corresponding to the energy ε_{max} at normal incidence, w is the normalized energy, ε_{thr} is the secondary emission threshold incident energy must exceed for emission to occur, k_{sw} is a surface smoothness parameter similar to k_s and was also set to 1 (both can vary between 0 for rough surfaces and 2 for polished surfaces). The secondary electrons are generated in the model according to Maxwellian distribution with 2 eV temperature.

In addition to the true secondary electron emission described by the expressions above it is important to take into consideration the reflection and scattering of the primary electrons. The main expected feature of the reflected and scattered electrons is their high energy with respect to the secondary electrons. In the described simulations we assume that 10% of the primary electrons are reflected from the surfaces so the normal component of the incident particle's velocity has its sign reversed. Another 10% of the incident particles are assumed to be scattered, i.e. all components of the particle's velocity are scaled by uniform (0, 1) random values keeping total energy unchanged. Thus 20% of the incident particles are returned to the discharge volume and the summary secondary electron yield is given by:

$$\delta_{sum} = \delta \cdot 0.8 + 0.2 . \quad (4)$$

In order to define the constants δ_{max}, ε_{max}, ε_{thr} for all the used materials we have analyzed experimental data available in literature [20 - 22].

It is well known that the secondary electron yield from a surface is highly dependent not only on the surface material but also on the surface condition (machining, contamination) [20]. Taking into account that the ε_{max} parameters for materials used in the present work are quite close and there is the significant uncertainty caused by the surface quality we defined ε_{max} = 300 eV for all the researched cases. The threshold energy was 0 eV for all the materials. Zero threshold energy may look non-physical; however, it allows satisfactory fit of the experimental data. Thus the only variable parameter in the used here secondary emission description is the δ_{max}. Since the δ_{max} for aluminium, steel and graphite is approximately 3.6, 1.7, 1 respectively, the calculations were conducted with δ_{max} in the range 0-6.

2.2. SIMULATION RESULTS

The results of systematic calculations are shown in the Fig. 3 in comparison with the experimental data. The simulations were performed for low pressures (30…300 mTorr) in the RF voltage range 80…500 V. A number of breakdown curves have been calculated for different secondary *e-e* emission yields.

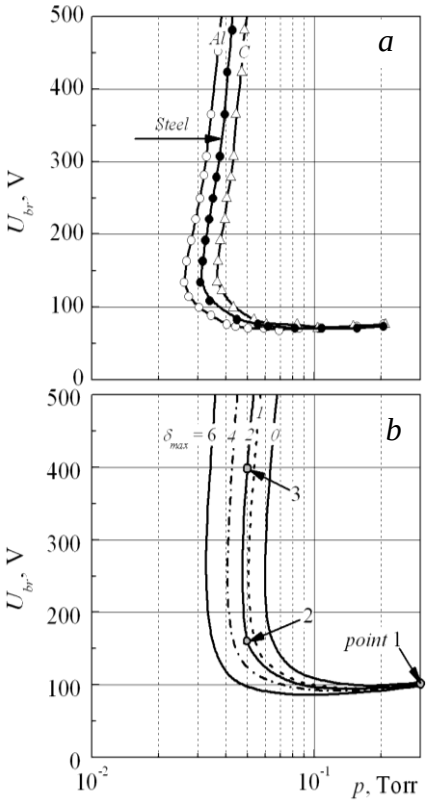

Fig. 3. Breakdown curves for different top electrode materials: a) experimental data, b) simulation results

One can see from the Fig. 3 that the simulation results are qualitatively consistent with the experimental data. All the breakdown curves demonstrate multivalued dependence at lowest pressures and coinciding right-hand branches. Similarly to the experimental curves the calculated dependences are shifted to the left and a bit down with δ_{max} growth.

The direct comparison of the experimental breakdown curve for aluminium with the theoretical curves shows the best fit corresponds to δ_{max} = 6 (Fig. 4). However, so high value of δ_{max} looks unlikely even taking into account impurities of the aluminium surface and its oxidization. General analysis for all the used materials shows that all the theoretic curves are slightly shifted to the right in relation to the corresponding experimental curves. The right-hand branches of the theoretic curves are approximately 20 V higher then the experimental.

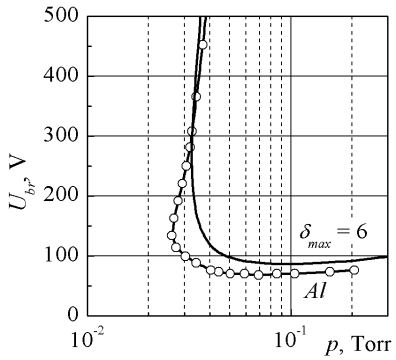

Fig. 4. Comparison of the experimental breakdown curve for aluminium with the theoretical curve with δ_{max}= 6

3. DISCUSSION

Thus, the results of experimental and theoretical investigation prove the significant influence of the electrode material on the RF discharge breakdown curve. Since the model accounted for *e-e* emission only and the simulation results are qualitatively consistent with the experimental data, we can make a conclusion about definitive role of the *e-e* emission in the RF discharge breakdown. As it was mentioned in introduction, one of the main purposes of the present paper is to clarify the physical mechanism of the influence of the secondary *e-e* emission on the RF gas breakdown.

For the detailed examination of the secondary electron influence on the discharge ignition we have carried out detailed calculations of the electron ensemble parameters depending on the phase of the applied RF voltage. In the figures below the sinusoid of the RF voltage applied to the bottom electrode is shown for reference, the vertical lines show the main phases of the RF oscillations: minimum, maximum and zeros. For comparison of pressure and voltage impact on the RF breakdown process we have chosen three characteristic points (see Fig. 3,b) at the breakdown curve for δ_{max} = 2: one at high pressure (point 1: p = 300 mTorr, U_{br} = 102 V), and two in the ambiguity region at the same low pressure p = 50 mTorr but with different breakdown voltages (point 2: U_{br} = 160 V; point 3: U_{br} = 400 V).

Let us consider first the dynamic balance of electrons in the discharge chamber. Dependences of the number of electrons in the chamber volume on the RF voltage phase are presented in Fig. 5 for the three characteristic points.

It is seen that the peaks of the curves correspond to the maximum absolute values of the RF electrode potential. Asymmetry of the peaks appears due to the asymmetry of the electrodes. The RF voltage decrease or the pressure increase reduces the electron number oscillation amplitude and the curve asymmetry. We should also mention the existence of a small delay of the maximum number of electrons with respect to the extrema of the sinusoid.

The analysis of the secondary electron creation requires knowledge of the primary electron current dynamics. In the Fig. 6 the dependences of the electron current to the potential electrode on the RF voltage phase are presented for the three characteristic points of the breakdown curve.

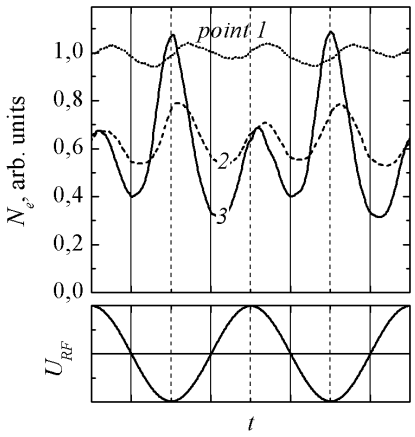

Fig. 5. Dependences of the number of electrons in the chamber volume on the RF voltage phase for the three characteristic points of the RF breakdown curve (see Fig. 3)

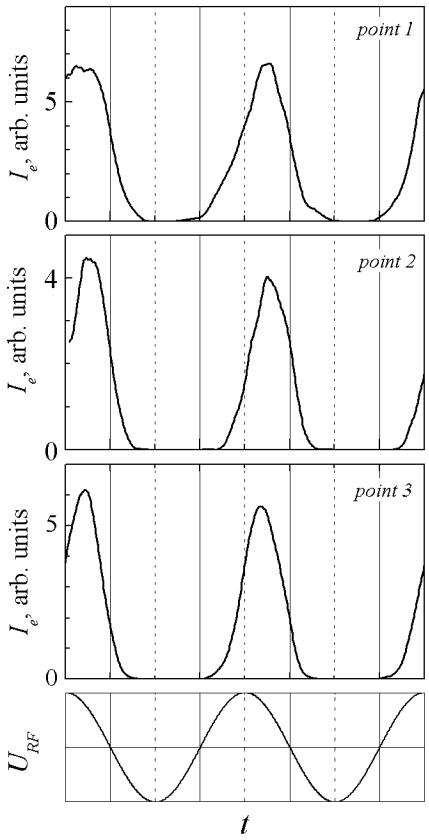

Fig. 6. Dependences of the electron current to the potential electrode on the RF voltage phase for the three characteristic points of the breakdown curve (see Fig.3)

The figure shows that the electrons hit the electrode by pulses mainly in phase of positive voltage peak. In the intervals between the pulses the electron current is essentially zero. As can be seen from the Fig. 6 there exists a region of nonzero electron current at the beginning of the half-cycle with negative electrode voltage, when the primary electrons reach the electrode in spite of the retarding electric field. Just during this time period all the secondary electrons escape from the electrode surface to the chamber volume, thus increasing the number of electrons in the discharge gap. From the Fig. 6 the conclusion can be made that only a small fraction of primary electrons can originate the secondary

electrons which may enter the volume of the chamber. Thus, despite the high values of the electron-impact secondary emission yield in comparison to the yields of other kinds of electron emission the efficiency of the secondary electron utilization in the breakdown process is quite low, so the importance of contributions of the different electron emission processes is under question.

In order to clarify the reason for the primary electron current existence despite the retarding electric field the electron distributions by *z* component of velocity were calculated. Such functions averaged over the chamber volume are shown in Fig. 7,a for the point 2 of the breakdown curve at the various phases of RF oscillations. The figure shows that at the moments of maximum value of the electric field the distribution function exhibits the presence of directed collective motion of electrons along with sufficiently large random component while at zero-field moments the distribution function is mostly symmetric.

In the Fig. 7,b the distribution functions are replotted in logarithmic scale on vertical axis with v_z represented in units of kinetic energy. One can see that the distributions at zero-field moments are surprisingly Maxwellian with characteristic temperature 8 eV.

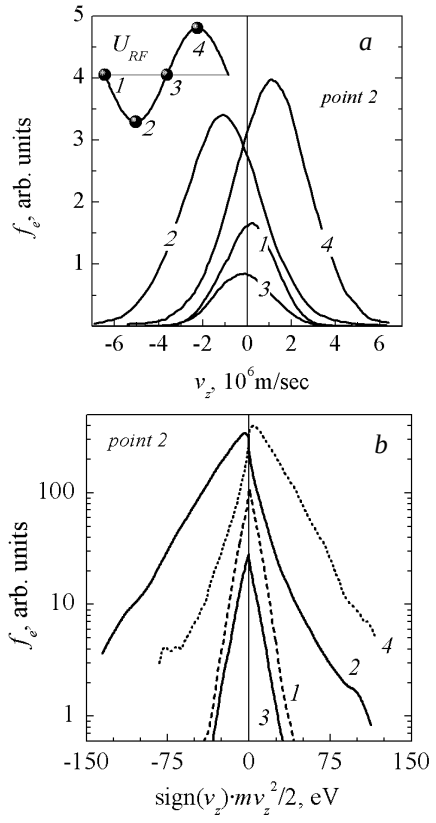

Fig. 7. Electron distributions by z component of velocity averaged over the chamber at the various phases of RF oscillations (a). The same distributions replotted in different scales. The curve numbers correspond to the points on the sinusoid plotted topmost (b)

Thus, after the termination of the field there is a rapid randomization of the electron motion, the electrons quickly "forget" the direction of movement without significant loss of energy. This looks natural taking into account the electron-atom collision frequency is at least an order of magnitude higher then the driving frequency, even at the lowest pressures. The majority of electrons at zero-field moments are low-energy, so their collisions with the argon atoms are elastic leading to significant change of the electron motion direction with almost conserved kinetic energy. Therefore, just after the electric field direction reversal the electrons can move against the field due to the thermal random motion, as opposed to the multipactor discharge, where the major role is played by the inertial motion of the electrons [14 - 16].

CONCLUSIONS

Thus, in the present paper the influence of the electron impact secondary electron emission on the RF gas breakdown has been researched experimentally and theoretically with use of PIC simulation. The experiments and simulations are conducted in the discharge chamber with asymmetric electrodes which is frequently used in technological applications. As a result, the physical mechanism of secondary electron participation in the RF breakdown has been revealed. It has been shown that the primary electron flow to the electrode against the electric field is provided due to chaotic thermal motion of the electrons rather than inertial motion as in the multipactor discharge.

REFERENCES

1. C. Gutton, S.K. Mitra and V. Ylostalo. Sur la decharge a haute frequence dans les gaz rarefies // *Comptes rendus Acad. Sci.* 1923, № 176, p. 1871-1874.
2. J. Thomson. The high-frequency glow discharge. // *Philosophical Magazine.* 1937, № 23, p. 1-19.
3. S. Githens. The influence of discharge chamber structure upon the initiating mechanism of the high frequency discharge// *Physical Review.* 1940, № 57, p. 822-828.
4. D.H. Hale. The breakdown of gases in high frequency electrical fields // *Physical Review.* 1948, № 73, p. 1046-1052.
5. T Kihara. The mathematical theory of electrical discharges in gases // *Reviews of Modern Physics.* 1995, № 224, p. 45-61.
6. S.M. Levitskii // *Soviet Physic-Technical Physics.* 1958, № 2, p. 887.
7. B. Thompson, H. Sawin. Comparison of measured and calculated SF_6 breakdown in rf electric fields //*Journal of Applied Physics.* 1986, № 60, p. 89-94.
8. V.A. Lisovsky, V.D. Yegorenkov. Low-pressure gas breakdown in combined fields // *Journal of Physics D: Applied Physics*. 1994, № 27, p. 2340-2348.
9. H.B. Smith, C. Charles and R.W. Boswell. Breakdown behavior in radio-frequency argon discharges // *Physics of Plasmas*. 2003, № 10, p. 875-881.
10. V. Lisovskiy, S. Martins, K. Landry, D. Douai, J.-P. Booth, V. Cassagne, V. Yegorenkov. The effect of discharge chamber geometry on the ignition of low-pressure rf capacitive discharges // *Physics of Plasmas*. 2005, № 12, p. 1-8.
11. V. Lisovskiy, K. Landry, D. Douai, J.-P. Booth, V. Cassagne, V. Yegorenkov. Electron drift velocity in argon, nitrogen, hydrogen, oxygen and ammonia in strong electric fields determined from rf break-

down curves // *Journal of Physics D: Applied Physics.* 2006, № 39, p. 660-665.
12. V. Lisovskiy, K. Landry, D. Douai, J.-P. Booth, V. Cassagne, V. Yegorenkov. Similarity law for RF breakdown // *Europhysics Letters.* 2008, № 82, p. 1-5.
13. M. Radmilovic-Radjenovic and J.K. Lee. Modeling of breakdown behavour in radio-frequency argon discharges with improved secondary emission model *// Physics of Plasmas*. 2005, № 12, p. 063501-8.
14. J.R.M. Vaughan. Multipactor *// IEEE Trans. on Plasma Science.* 1988, № 35, p. 1172-1180.
15. A.J. Hatch, H.B. Williams. Multipacting modes of high-frequency gaseous breakdown // *Physical Review.* 1958, № 112, p. 681-685.
16. F. Hohn, W. Jacob, R. Beckmann and R. Wilhelm. The transition of a multipactor to a low-pressure gas discharge // *Physics of Plasmas.* 1997, № 4, p. 940-944.
17. J.R.M. Vaughan. Secondary emission formulas // *IEEE Transactions on Plasma Science*. 1993, № 40, p. 830.
18. J.P. Verboncoeur, A.B. Langden and N.T. Gladd. An object-oriented electromagnetic PIC code // *Computer Physics Communications.* 1995, № 87, p. 199-211.
19. J.R.M. Vaughan. A new formula for secondary emission yield // *IEEE Transactions on Electron Devices.* 1989, № 36, p. 1963-1967.
20. V. Baglin, J. Bojko, O. Grobner, B. Henrist, N. Hilleret, C. Scheuerlein and M. Taborelli. The secondary electron yield of technical materials and its variation with surface treatments // *Proc. 7th European Particle Accelerator Conference (Vienna: Austria)*. 2000, p. 217-221.
21. R.E. Kirby. Instrumental effects in secondary electron yield and energy distribution measurements *// Proc. 31st ICFA Advanced Beam Dynamics Workshop on Electron-Cloud Effects "ECLOUD'04" (Napa: California)*. 2004, p. 107-112.
22. F. Le Pimpec, R.E. Kirby, F.K. King and M. Pivi. Electron conditioning of technical aluminium surfaces: Effect on the secondary electron yield // *Journal of Vacuum Science and Technology A*. 2005, № 23, p. 1610.

Article received 26.03.2013.

ВЛИЯНИЕ ВТОРИЧНОЙ ЭЛЕКТРОННОЙ ЭМИССИИ НА ВЧ-ПРОБОЙ ГАЗА

А.Н. Дахов, С.В. Дудин

Изучено влияние вторичной электронной эмиссии на ВЧ-пробой газа для разрядной камеры с асимметричными электродами. Проведены экспериментальные исследования и численные расчеты с использованием метода PIC (particle-in-sell). Объяснен физический механизм участия вторичных электронов в ВЧ-пробое газа.

ВПЛИВ ВТОРИННОЇ ЕЛЕКТРОННОЇ ЕМІСІЇ НА ВЧ-ПРОБІЙ ГАЗУ

О.М. Дахов, С.В. Дудін

Вивчено вплив вторинної електронної емісії на ВЧ-пробій газу для розрядної камери з асиметричними електродами. Проведено експериментальні дослідження та чисельні розрахунки з використанням методу PIC (particle-in-sell). Пояснений фізичний механізм участі вторинних електронів в ВЧ-пробої газу.